A Mode-Matching Solution for Scattering from a Large Isosceles Right Triangle Groove in PEC Plane

Mehdi Bozorgi

Department of Electrical Engineering, Faculty of Engineering, Arak University, Arak, Iran
*corresponding author, E-mail: M-Bozorgi@araku.ac.ir

Abstract

An efficient mode-matching manner involving physical optics approximation is planned for scattering from a large Isosceles Right Triangular Groove (IRTG) in an infinite Perfect Electric Conductor (PEC) plane. By considering two synthetic PEC walls over the groove, the tangential fields inside and outside the groove are expanded as the sums of infinite harmonics modes. These modes are matched over the IRTG and consequently, a system of linear equations is constructed for the expansion coefficients. The examination of the results shows that this method is not appropriate for grooves with a width smaller than the wavelength. Instead, for a large IRTG, it can reduce simulation time considerably and is in good agreement with time-consuming numerical methods such as the Finite Element Method (FEM) and the Method of Moment (MoM). The effects of the angle of incidence and the groove width on the scattering signature are investigated, too.

1. Introduction

The evaluating of scattered waves from cavities is a primary subject in many applications such as Radar Cross Section (RCS) reduction and Non-Destructive Testing (NDT). Generally, radar cross-sectional studies on different open cavities provide valuable information that can be used for target classification and identification. Also, scattering by electrically large components with different and periodic shape is becoming increasingly important due to their high application in optics, light scattering, nanofabrication-based terahertz technology, microwave diffraction and spectroscopy [1-4].

A lot of research has been done on scattering from open cavities in the last decade [5-14]. Most of them have been tried to obtain scattered waves from a rectangular groove by using different methods. New techniques have been developed to compensate for the inefficiency and inaccuracy of general full-wave solvers. Accuracy and time efficiency are significant subjects in recent studies. In the literature [8], a reduction in computation time was achieved by using a hybrid technique. In [9], a direct integral equation solver (DIES) has been proposed for scattering by an arbitrary rectangular crack. Their approach solves a hyper singular integral equation quickly and accurately by a collocation method based on Chebyshev polynomials. In [10], the overlapping T-block method has been used to obtain an accurate closed-form expression for far-field scattered waves from a rectangular groove. Fourier transform technique for scattering from a large rectangular crack has also been reported in the literature [11].

There are few reports that have been tried to obtain the scattered fields by triangular grooves [12-14]. For TM-backscattering by an IRTG, The Fourier transform technique has been proposed in [12]. They obtained a closed-form equation to compute unknown series coefficients by residue calculus theorem. In [13], an efficient method for a general-shaped open cavity has been projected to analyze scattered waves in TM mode. Their method consists of dividing an open cavity into L number of layers, expanding the fields in the spectral domain, and matching on the adjacent layers. Ramahi and Alavikia suggested a numerical solution to compute scattered waves from an arbitrary cavity for both TM and TE polarization [14]. Their technique combines finite-element and the surface integral equation methods to reduce simulation time.

However, when the width of a groove is comparable to the wavelength of the incident waves or larger, numerical methods that mesh the object surface are often time-consuming and inefficient. In these types of numerical methods, when the width and depth of a groove increase, the computational time increases dramatically and thus, more memory requirements. In literature [11] and [8], two efficient methods based on Fourier transform and modal techniques have been projected to solve this problem for large rectangular grooves. In fact, there are basically two types of approach to solve the scattering problem for large cavities. The first type applies the high-frequency asymptotic techniques (for example physical optics approximation and shooting and bouncing rays method). Another type of method is known as the modal technique.

In this paper, without using complex mathematical concepts, an efficient solution for TE and TM-scattering from a 2-D large IRTG in an infinite PEC plane is suggested utilizing mode-matching and physical optics techniques. First, we replace the half-space above the IRTG with two parallel artificial PEC walls that make a semi-infinite waveguide [8]. Replacing the upper half-space with a parallel waveguide leads a proper physical approximation and considerably simplifies calculations. A comparison of results obtained by different methods demonstrates that this approximation has no significant effect on the accuracy of the results. To use the Mode-Matching technique, the tangential fields inside and outside the IRTG are expanded

using half range Fourier series. Mode-by-Mode fields matching across the groove leads to a system of linear equations that its coefficients can be calculated analytically. The linear system can be stated in matrix form and solved by finding the inverse of an $N\times N$ matrix that can be a time-consuming process. Finally, some examples are presented and their results are compared with usual numerical methods such as MoM and FEM. we use this approach to investigate the effects of the width of IRTG and the angle of incidence on two-dimensional scattering patterns.

2. Problem description

Assume a plane wave with arbitrary polarisation illuminates a 2-D large IRTG filled with ε_2 and μ_2 as shown in Fig.1

$$H_z^i, E_z^i = \hat{z}e^{jk_1((x-\frac{W}{2})\cos\varphi_0 + y\sin\varphi_0)} \quad \varphi_0 \in (0,\pi). \tag{1}$$

where k_1 , φ_0 and W are the free space propagation constant , the angle of incidence and the width of the groove, respectively. The transverse electric field E_z^{IRT} and magnetic field H_z^{IRT} in a isosceles right triangular waveguide can be obtained as the sum of all possible propagation waves [15], i.e.,

$$H_z^{IRT}, E_z^{IRT} = \hat{z}\sum_{m=0}^{M}\sum_{i=1}^{I} E_{mi}, H_{mi}\, e^{-jk_0\hat{k}_i.\vec{r}} \tag{2}$$

Where M and I are the number of modes and the total number of wave vectors, respectively, $\hat{r} = x\hat{X} + (y+W)\hat{Y}$ and $\hat{k}_i$ is the incident unit wave vector. For the IRTG shown in Fig.1, I=8 and transverse wave propagation vectors are determined as following [15]

$$\hat{k}_{i=1,2,\ldots 8} = \mp\alpha\hat{X} \mp \beta\hat{Y} \tag{3}$$

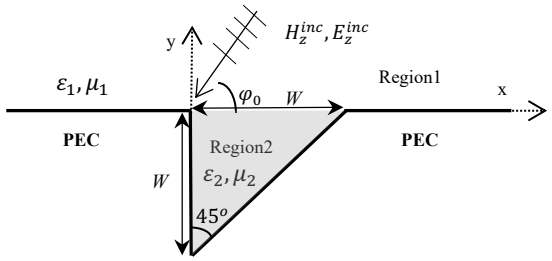

Fig.1. The geometry of 2-D IRTG filled with a material ε_2, μ_2

Where α and β are the propagation constant in the direction of the two coordinate axes x and y. Thus H_z^{IRT} and E_z^{IRT} for TE and TM polarizations are given as:

$$H_z^{IRT}, E_z^{IRT} = \vec{z}\sum_{m=0}^{M}\sum_{i=1}^{8} E_{mi}, H_{mi}\, e^{jk_0(\mp\alpha x \mp\beta(y+W))} \tag{4}$$

We apply the following the boundary conditions to the IRTG shown in Fig.1,

$$\begin{cases} E_z^{IRT} = 0, & on\ x = 0\ and\ \ y = x - W \\ \dfrac{\partial H_z^{IRT}}{\partial x} = 0 & on\ x = 0 \\ \dfrac{\partial H_z^{IRT}}{\partial y} = \dfrac{\partial H_z^{IRT}}{\partial x} & on\ \ y = x - W \end{cases}$$

and then the mode functions for TE and TM modes are obtained as:

$$E_z^{IRT} = \sum_{n=0}^{\infty} E_n^I[\sin(\alpha_n x)\sin(\beta_n(y+W)) - \sin(\beta_n x)\sin(\alpha_n(y+W))], \quad \text{TM Mode} \tag{5}$$

and

$$H_z^{IRT} = \sum_{n=0}^{\infty} H_n^I[\cos(\alpha_n x)\cos(\beta_n(y+W)) + \cos(\beta_n x)\cos(\alpha_n(y+W))], \quad \text{TE Mode} \tag{6}$$

Where $k_2 = \sqrt{\alpha_n^2 + \beta_n^2}$, and E_m^I and H_m^I are unknown coefficients. The equations (5) and (6) are valid for all values α_n and β_n [12]. Thus, the eigenvalues α_n and β_n can be selected similar to an isosceles right triangular waveguide i.e., $\alpha_n = \frac{n\pi}{W}$ and $\beta_n = \sqrt{k_2^2 - \alpha_n^2}$.

To obtain mode functions in the half-space above the IRTG, we replace the upper half-space with two parallel PEC walls, as shown in Fig. 2 [8]. This approximation allows us to find simpler expressions for scattering from a large groove while the accuracy of the results does not change that much.

The electromagnetic fields in the artificial waveguide outside the groove vanish along the axis of y (+y direction). Therefore, the transverse magnetic H_z^{Up} and electric field E_z^{Up} in the artificial waveguide can be expanded as:

$$E_z^{Up} = \sum_{n=1}^{\infty} E_n^U\, sin(\alpha_n x)e^{-\gamma_n y} \quad \text{TM Mode} \tag{7}$$

and

$$H_z^{Up} = \sum_{n=1}^{\infty} H_n^U\, cos(\alpha_n x)e^{-\gamma_n y} \quad \text{TE Mode} \tag{8}$$

where $\gamma_n = \sqrt{\beta_n^2 - k_2^2}$ and E_m^U , H_m^U are unknown coefficients that should be calculated. We suppose that the width of the groove is large enough to use high-frequency asymptotic techniques like physical optics approximation.

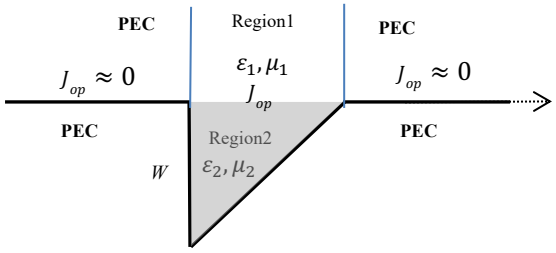

Fig.2. Substituting upper half-space above a 2-D large IRTG with two parallel PEC walls

Given the structure of the problem shown in Fig.2, the physical optic current $\hat{J}_{op}$ can be expressed as $\hat{J}_{op} = 2\hat{y} \times \hat{H}^{i}_{tan}$. Where $\vec{H}^{i}_{tan}$ denotes to the incidence tangential magnetic field over an open cavity. Due to the continuity of the tangential fields on the IRTG, the boundary conditions at $y = 0$ are given by

$$\hat{H}^{U}_{tan} - \hat{H}^{IRT}_{tan} = \hat{J}_{op},\ \hat{E}^{U}_{tan} - \hat{E}^{IRT}_{tan} = 0\,, \qquad y = 0 \tag{9}$$

Where

$$\hat{H}_{tan} = \begin{cases} H_x, & \text{TM Mode} \\ H_z, & \text{TE Mode} \end{cases} \text{ and } \hat{E}_{tan} = \begin{cases} E_x, & \text{TE Mode} \\ E_z, & \text{TM Mode} \end{cases}$$

3. Appling Mode-Matching method

In section 2, the tangential fields inside and outside the IRTG were represented as a sum of infinite harmonic modes. Mode-by-Mode tangential fields matching across the IRTG leads to an infinite system of linear equations for each polarization.

3.1. TM-Polarization

The x-components of the magnetic field inside the groove (H^{IRT}_{x}) and the artificial waveguide outside the IRTG (H^{Up}_{x}) can be written as:

$$H^{IRT}_{x}(x,y) = \frac{-1}{j\omega\mu_2}\frac{\partial E^{IRT}_{z}(x,y)}{\partial y} = \frac{-1}{j\omega\mu_2}\sum_{n=1}^{\infty} E^{I}_{n}[\beta_n \sin(\alpha_n x)\cos(\beta_n(y+W)) - \alpha_n \sin(\beta_n x)\cos(\alpha_n(y+W))] \tag{10}$$

and

$$H^{Up}_{x} = \frac{j}{\omega\mu_1}\sum_{n=1}^{\infty} E^{U}_{n}\,\gamma_n sin(\alpha_n x) e^{-\gamma_n y} \tag{11}$$

moreover, the x-component of the incident plane wave is

$$H^{i}_{x} = \frac{\sin\varphi_0}{\eta}\, e^{jk_1((x-\frac{W}{2})\cos\varphi_0 + y\sin\varphi_0)} \tag{12}$$

where $\eta = 120\pi$ is the free space impedance. We apply boundary conditions (9) to tangential fields at y=0 and construct two independent equations as follows:

$$\frac{-1}{j\omega\mu_2}\sum_{n=1}^{\infty} E^{I}_{n}\,[\beta_n \sin(\alpha_n x)\cos(\beta_n W) - \alpha_n \sin(\beta_n x)\cos(\alpha_n W)] - \frac{j}{\omega\mu_1}\sum_{n=1}^{\infty} E^{U}_{n}\,\gamma_n sin(\alpha_n x) = 2\frac{\sin\varphi_0}{\eta}\, e^{jk_1(x-\frac{W}{2})\cos\varphi_0} \tag{13}$$

and

$$\sum_{m=0}^{\infty} E^{I}_{m}\sin(\alpha_n x)\sin(\beta_n W) = \sum_{n=1}^{\infty} E^{U}_{m}\, sin(\alpha_n x) \tag{14}$$

To utilize the Mode-Matching technique, the functions $\sin(\beta_n x)$ and $\exp\left(jk_1\left(x-\frac{W}{2}\right)\cos\varphi_0\right.$ in equation (13) should be expanded using half range Fourier sine series (basis function $sin(\alpha_n x)$) as:

$$\sin(\beta_n x) = \sum_{m=1}^{\infty} a_{mn}\ sin(\alpha_m x) \tag{15}$$

and

$$\frac{2\sin\varphi_0}{\eta}\, e^{jk_1(x-\frac{W}{2})\cos\varphi_0} = \sum_{n=1}^{\infty} b_n\ sin(\alpha_n x) \tag{16}$$

The coefficients a_m and b_m in (15) and (16) can be easily calculated analytically:

$$a_{mn} = \frac{2}{W}\int_0^W sin(\alpha_m x)\sin(\beta_n x)dx = \frac{sin(m\pi-\beta_n W)}{m\pi-\beta_n W} - \frac{sin(m\pi+\beta_n W)}{m\pi+\beta_n W} \tag{17}$$

and

$$b_n = \frac{4\sin\varphi_0}{\eta W}\int_0^W sin(\alpha_n x)\, e^{jk_1(x-\frac{W}{2})\cos\varphi_0}dx = 2n\pi sin\varphi_0 \frac{e^{-j\frac{k_1 W}{2}\cos\varphi_0} - (-1)^n e^{j\frac{k_1 W}{2}\cos\varphi_0}}{(n\pi)^2 + (jk_1 W\cos\varphi_0)^2} \tag{18}$$

After replacing (15) and (16) in (13), the modes in the equations (13) and (14) are matched and two linear equations are constructed for unknown parameters E^{I}_{n} and E^{U}_{n} as follows:

$$E^{I}_{n}\sin(\beta_n W) = E^{U}_{n} \tag{19}$$

and

$$\frac{j}{\omega\mu_2}[\beta_n\cos(\beta_n W)E^{I}_{n} - \sum_{m=1}^{\infty} E^{I}_{m}a_{nm}\alpha_m cos(\alpha_m W)] - \frac{j\gamma_n E^{U}_{n}}{\omega\mu_1} = b_n \tag{20}$$

We substitute $E^{I}_{n}\sin(\beta_n W)$ in (19) for E^{U}_{n} in the equation (20) to obtain the following equation as:

$$\frac{j\beta_n}{\omega\mu_2}\cos(\beta_n W)E^{I}_{n} - \frac{j}{\omega\mu_2}\sum_{m=1}^{\infty} a_{nm}\alpha_m cos(\alpha_m W)\, E^{I}_{m} - \frac{j\gamma_n}{\omega\mu_1}\sin(\beta_n W)E^{I}_{n} = b_n \tag{21}$$

The infinite sum in (13) and (21) can be truncated at $m = n = M$ and consequently, a system of linear equations in M unknowns is constructed. We represent it in the following matrix form as:

$$\begin{bmatrix} b_0 \\ b_1 \\ \cdot \\ \cdot \\ b_M \end{bmatrix} = \begin{bmatrix} K_{00} & K_{01} & \cdots & K_{0M} \\ K_{10} & K_{11} & & K_{1M} \\ \vdots & & \ddots & \vdots \\ K_{M0} & K_{M1} & \cdots & K_{MM} \end{bmatrix} \begin{bmatrix} E_0^I \\ E_1^I \\ \cdot \\ \cdot \\ E_M^I \end{bmatrix} \quad (22)$$

where the matrix elements K_{nm} are calculated analytically as:

$$K_{nm} = \begin{cases} \frac{j\beta_m}{\omega\mu_2}\cos(\beta_m W) - \frac{j\gamma_m}{\omega\mu_1}\sin(\beta_m W) \\ -\frac{ja_{mm}\alpha_m}{\omega\mu_2} cos(\alpha_m W), & m = n \\ \\ -\frac{ja_{nm}\alpha_m}{\omega\mu_2} cos(\alpha_m W), & m \neq n \end{cases} \quad (23)$$

3.2. TE-Polarization

We can repeat the above procedure for TM polarization. Therefore, First, the boundary conditions (9) are applied to the tangential fields E_x^{IRT}, H_z^{IRT}, E_x^U and H_z^U over the IRTG at *y=0* to construct two following equations as:

$$\sum_{n=0}^{\infty} H_n^I[\cos(\alpha_n x)\cos(\beta_n W) + \cos(\beta_n x)\cos(\alpha_n W)]$$
$$-\sum_{n=1}^{\infty} H_n^U cos(\alpha_n x) = 2e^{jk_1(x-\frac{W}{2})\cos\varphi_0} \quad (24)$$

and

$$\frac{1}{j\omega\varepsilon_2}\sum_{n=0}^{\infty} H_n^I\beta_n\cos(\alpha_n x)\sin(\beta_n W)$$
$$= \frac{1}{j\omega\varepsilon_1}\sum_{n=0}^{\infty} H_n^U\gamma_n\cos(\alpha_n x) \quad (25)$$

Now, the functions $\cos(\beta_n x)$ and $\exp\left(jk_1\left(x-\frac{W}{2}\right)\cos\varphi_0\right)$ in (24) are expanded using the base function $\cos(\alpha_n x)$. Thus we take:

$$\cos(\beta_n x) = \sum_{m=0}^{\infty} a_{mn}\ cos(\alpha_m x) \quad (26)$$

and

$$2e^{jk_1(x-\frac{W}{2})\cos\varphi_0} = \sum_{n=0}^{\infty} b_n\, cos(\alpha_n x) \quad (27)$$

Where the expansion coefficients a_{mn} and b_n are given by

$$a_{mn} = \frac{\varepsilon_m}{W}\int_0^W cos(\alpha_m x)\cos(\beta_n x)dx =$$

$$\begin{cases} \frac{sin(m\pi-\beta_n W)}{m\pi-\beta_n W} + \frac{sin(m\pi+\beta_n W)}{m\pi+\beta_n W}, & m \neq 0 \\ \frac{sin(\beta_n W)}{\beta_n W}, & m = 0 \end{cases} \quad (28)$$

and

$$b_n = \frac{2\varepsilon_n}{W}\int_0^W cos(\alpha_n x)\, e^{jk_1(x-\frac{W}{2})\cos\varphi_0}dx =$$
$$jk_1 W\cos\varphi_0\varepsilon_n\frac{e^{-j\frac{k_1 W}{2}\cos\varphi_0} - (-1)^n e^{j\frac{k_1 W}{2}\cos\varphi_0}}{(n\pi)^2 + (jk_1 W\cos\varphi_0)^2} \quad (29)$$

where $\varepsilon_n = 1$ if $n = 0$ otherwise $\varepsilon_n = 2$. After substituting (26)-(27) in (24), for each mode, we can obtain two independent equations as follow:

$$\frac{\beta_n}{j\omega\varepsilon_2}\sin(\beta_n W)H_n^I = \frac{\gamma_n}{j\omega\varepsilon_1}H_n^U \quad (30)$$

and

$$\cos(\beta_n W)\, H_n^I - \sum_{m=1}^{\infty} H_m^I\cos(\alpha_m W)\, a_{nm} - H_n^U = b_n \quad (31)$$

By substituting the equations (30) for H_n^U in the equation (31), an infinite system of linear equations is constructed for the unknown coefficients H_m^I as:

$$\cos(\beta_n W)\, H_n^I - \frac{\beta_n\varepsilon_1}{\gamma_n\varepsilon_2}H_n^I - \sum_{m=1}^{\infty} H_m^I\cos(\alpha_m W)\, a_{nm} = b_n \quad (32)$$

We truncate the infinite sums at *m=n=M*. Finally, the matrix form of equation (32) is given below

$$\begin{bmatrix} b_0 \\ b_1 \\ \cdot \\ \cdot \\ b_M \end{bmatrix} = \begin{bmatrix} L_{00} & L_{01} & \cdots & L_{0M} \\ L_{10} & L_{11} & & L_{1M} \\ \vdots & & \ddots & \vdots \\ L_{M0} & L_{M1} & \cdots & L_{MM} \end{bmatrix} \begin{bmatrix} H_0^I \\ H_1^I \\ \cdot \\ \cdot \\ H_M^I \end{bmatrix} \quad (33)$$

where the matrix elements L_{nm} are computed as:

$$L_{nm} = \begin{cases} \cos(\beta_m W) - \frac{\beta_m\varepsilon_1}{\gamma_m\varepsilon_2} - \cos(\alpha_m W)\, a_{mm}, & m = n \\ \\ -\cos(\alpha_m W)\, a_{nm}, & m \neq n \end{cases} \quad (34)$$

3.3. 2-D RCS calculation

The coefficients H_n^I (TE case) and E_n^I (TM case) are obtained by finding the inverse of the square matrixes in (22) and (33) and then coefficients H_n^U and E_n^U can be determined certainly. Now, we can compute the far-field H_z^s and E_z^s easily by knowing the tangential fields over the groove(y=0) as [9]:

$$H_z^s = -\hat{f}(\rho)y_1\int_0^W E_x(x', y'=0)e^{jk_1 x'\cos\varphi_0}\, dx' \quad (35)$$

and

$$E_z^s = \hat{f}(\rho)\sin\varphi\int_0^W E_z(x', y'=0)e^{jk_1 x'\cos\varphi_0}\, dx' \quad (36)$$

Where

$$\hat{f}(\rho) = \hat{z}e^{-jk_0\rho}e^{j\frac{\pi}{4}}\sqrt{\frac{k_1}{2\pi\rho}} \quad (37)$$

By replacing (7) and (8) in (34) and (35) we have:

$$H_z^S = -\hat{f}(\rho)y_1 \sum_{m=1}^{\infty} H_m^U \int_0^W cos(\alpha_m x)e^{jk_1 x' \cos\varphi_0}\, dx' \quad (38)$$

and

$$E_z^S = \hat{f}(\rho)\sin\varphi \sum_{m=1}^{\infty} E_m^U \int_0^W sin(\alpha_m x)e^{jk_1 x' \cos\varphi_0}\, dx' \quad (39)$$

The integrals in (38) and (39) have an analytic solution like the formulas (18) and (29). Finally, the 2-D radar cross-section is computed as follow:

$$\sigma_{TE}^{2D} = \lim_{\rho\to\infty} 2\pi\rho \frac{|H_z^S|^2}{|H_z^i|^2} \quad (40)$$

and

$$\sigma_{TM}^{2D} = \lim_{\rho\to\infty} 2\pi\rho \frac{|E_z^S|^2}{|E_z^i|^2} \quad (41)$$

4. Results

In this section, some comparisons are presented to show the validity and accuracy of the proposed method. The method is verified by comparison with Finite Element Method (FEM) and Method of Moment (MoM) solutions obtained using commercial software FEKO and HFSS respectively and then used to investigate the effects of the problem parameters on the scattering patterns.

Fig. 3 illustrates variations of the tangential electric fields E_x and E_z for TE and TM polarizations respectively, when x-position changes at y=0 for an IRTG (Fig.1) of $W = 4\lambda$ filled with a dielectric $\varepsilon_{r2} = 2.5 - j0.2$ and $\mu_{r2} = 1.8 - j0.1$. Also, the angles of incidence for TE and TM modes $\varphi_0 = 60^o$ and $\varphi_0 = 90^o$ have been selected respectively. These results are obtained by truncating the infinite series at *M*=16 in equations (21) and (31). More experiments show that the results converge fast when $N > \frac{2W}{\lambda_0}\sqrt{|\varepsilon_{r2}\mu_{r2}|}$ [8]. Here, we select $N = int[\frac{2W}{\lambda_0}\sqrt{|\varepsilon_{r2}\mu_{r2}|}] + 1$ to get better accuracy. Where $int[.]$ denotes the integer part of the argument. As shown in Fig. 3, the results are in good agreement with the numerical solutions of FEM and MoM.

The effect of the width of the IRTG on the echowidth at the normal incidence angle is shown in Figs. 4(a) and 4(b). In this example, the specification of the IRTG is similar to the previous example. Taking the FEM and MoM as the reference, it can be deduced from the results shown in Fig. 4 that the proposed procedure is just accurate for a wide IRTG. These results become invalid for an IRTG that its width is smaller than the wavelength of a plane wave ($W < \lambda$). However, we can say that these results are acceptable for $W = \lambda$ and as the groove widens, the results become more accurate. When the width of IRTG increases, the echowidth increases as well.

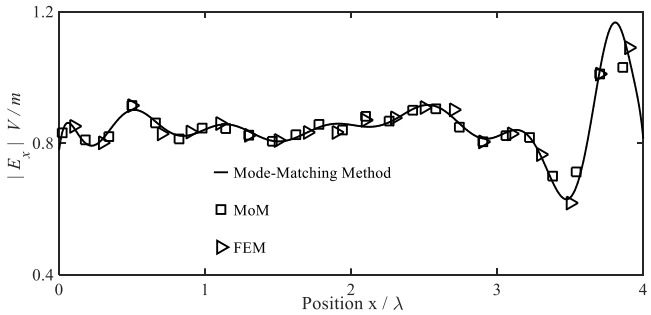

(a) For TE mode at $\varphi_0 = 60^o$

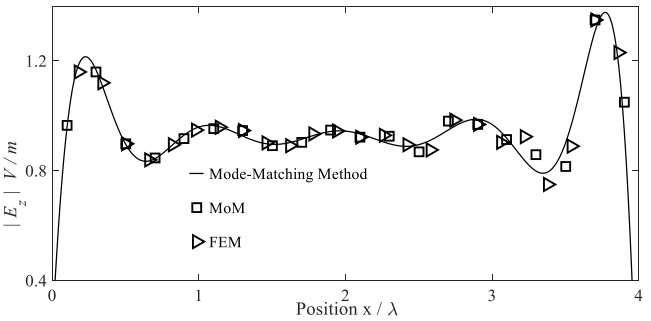

(b) For TM mode at $\varphi_0 = 90^o$

Fig.3. The distribution of the electric fields E_x and E_z over a filled IRTG at *y=0* ($\varepsilon_{r2} = 2.5 - j0.2$, $\mu_{r2} = 1.8 - j0.1$ and $\varepsilon_1 = \varepsilon_0, \mu_1 = \mu_0$) with $W = 4\lambda$. (a) TE mode, (b) TM mode.

As mentioned, the numerical methods that use meshing techniques are generally very time-consuming for large grooves. In such structures, the use of the suggested method can increase the computational speed significantly. To study the computational efficiency of the suggested method, we have measured the simulation time of each method used in Fig. 3. The simulation times for this method, MoM and FEM are measured about 100ms, 14min, and 23 min, respectively. As expected, there is a significant difference between the simulation times of this meshless method and the other numerical methods that mesh the surface of an object, including MoM and FEM. Consequently, while using this method is not suitable for a small groove, it can be reduced the simulation time for a large groove with the desired accuracy.

To determine the 2-D scattering signature of a large IRTG, we have plotted bistatic echowidth for various observation angles in the polar coordinate when $W = 2\lambda, 3\lambda, 4\lambda$ and 5λ at normal the incidence of angle ($\varphi_0 = 90^o$) for TE and TM modes. Figs. 5 shows, how the bistatic echowidth patterns change when the width of IRTG increases.

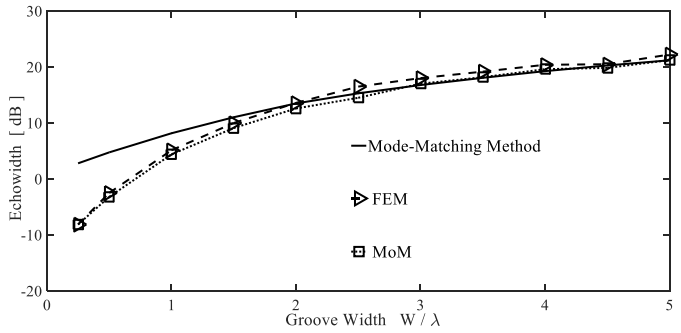

(a) TE mode

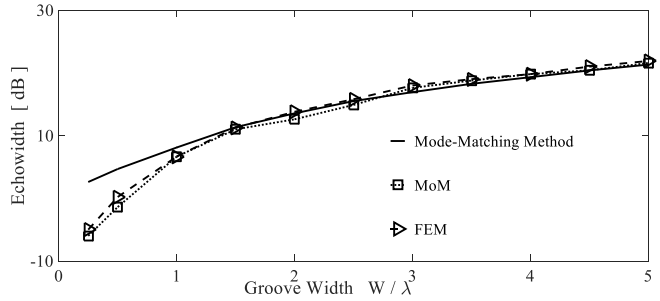

(b) TM mode

Fig.4. The echowidth of a dielectric-filled IRTG ($\varepsilon_{r2} = 2.5 - j0.2$, $\mu_{r2} = 1.8 - j0.1$ and $\varepsilon_1 = \varepsilon_0, \mu_1 = \mu_0$) at normal incidence angle for various groove widths. (a) TE mode, (b) TM mode.

An inspection of the results in Figs. 5 demonstrates that for TE and TM polarizations when the groove width increases, the side lobes increase and the width of the main lobes decreases while little energy is inserted to the main lobe. There is a direct relation between the width of an IRTG and the number of the side lobes. The number of side lobes for a groove width with an integer number of wavelengths $W = N\lambda$, equals $2N - 2$. At the normal incidence angle, the bistatic echowidth patterns for both modes are nearly symmetrical and the maximum scattering cross-section is observed in the vertical direction.

To examine the effect of the angle of incidence on scattering patterns, we have calculated the bistatic echowidth as shown in Fig. 6 for TM and TE modes. These results are obtained for a filled IRTG when $W = 4\lambda$ and $\varepsilon_{r2} = 2.5 - j0.2$, $\mu_{r2} = 1.8 - j0.1$ at the incidence angles $\varphi_0 = 30^o$, $\varphi_0 = 45^o$, $\varphi_0 = 60^o$ and $\varphi_0 = 90^o$. As can be seen in these figures, the maximum scattering happens in the incidence wave direction and the scattered power density on the side of the incidence angle is greater than the opposite. A study on the results shown in Figs. 5 and 6 demonstrates that the scattering signature directly related to the width of IRTG and the angle of incidence. At oblique incidence, the side lobes that are below the incidence angle ($\varphi < \varphi_0$) are broader than other side lobes. However, the side lobes become weaker and wider when the observation angle gets close to the groove surface.

It is noting that the solution described in this paper can be utilized to predict the scattering signature by variant electrically large structures.

$\varphi_0 = 90^o$	TE mode	TM mode
$W = 2\lambda$	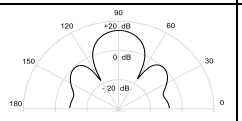	
$W = 3\lambda$	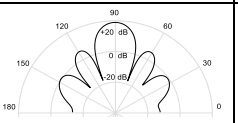	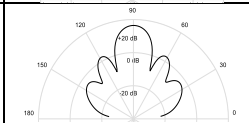
$W = 4\lambda$	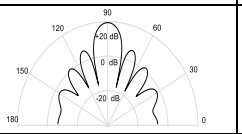	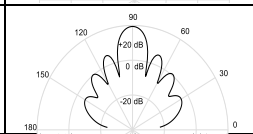
$W = 5\lambda$	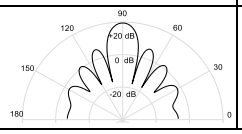	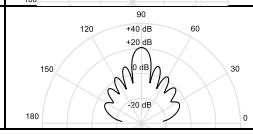

Fig.5. Bistatic echowidth patterns at $\varphi_0 = 90^o$ and $\varphi_0 = 60^o$ for the various IRTG widths $W = \lambda, 2\lambda, 3\lambda$, and$4\lambda$

$W = 4\lambda$	TE mode	TM mode
$\varphi_0 = 30^o$	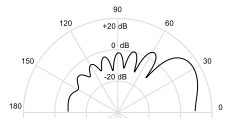	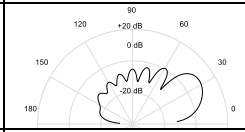
$\varphi_0 = 45^o$	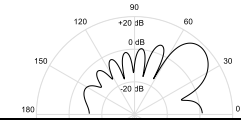	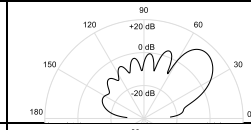
$\varphi_0 = 60^o$	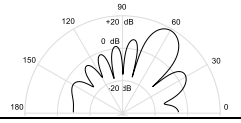	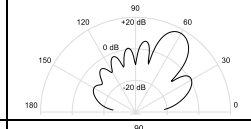
$\varphi_0 = 90^o$	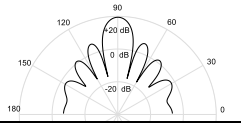	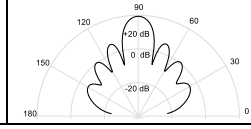

Fig.6. Bistatic echowidth patterns for $W = 4\lambda$ at various the angles of incidence $\varphi_0 = 30^o, 45^o, 60^o$and 90^o.

5. Conclusion

Scattering by a large IRTG in an infinite PEC plane was investigated using a simple yet effective method that is a combination of the mode-matching and physical optics techniques. The solution consists of replacing half-space above IRTG with two PEC walls, expanding the tangential fields inside and outside IRTG, matching modes over the groove and determining the coefficients of expansion via solving a system of linear equations. The suggested manner was verified by comparison with FEM and MoM solutions. The time-consuming and the limitation of the method and

the effects of the angle of incidence and the groove width on the scattering signatures of a large IRTG were examined. This method is not suitable for a groove width smaller than the wavelength. The simulation time of this method is considerably low and it can be utilized for scattering studies on electrically large structures that are important in many design analyses for such fields as light scattering, optical device, terahertz technology, sensing, and nano-technology.

References

[1] Alnaiemy, T. A. Elwi, N. Lajos, and T. Zwick, “A Systematic Analysis and Design of a High Gain Microstrip Antenna based on a Single EBG Layer,” IEEE INFOCOMMUNICATIONS JOURNAL, volume 10, pp. 1-9, December, 2018,

[2] A. Elwi and Y. Alnaiemy, “Nano-Scale Vee Yagi-Uda Antenna based Nano Shell-Silver Coated Silica for Tunable Solid State Laser Applications”, Diyala Journal of Engineering Sciences, volume 12, no. 1, pp: 85-93, January 2019,

[3] A. Elwi, “Toward Plasmonic UC-PBG Structures based SWCNTs for Optoelectronics Applications”, Diyala Journal for Pure Science, volume 14, issue 1, part 1, April 2018

[4] Palmer, C., Diffraction Grating Handbook, Newport Corporation, Rochester, NY (2004)

[5] K. Barkashli and J. L. Volakis, "TE scattering by a two-dimensional groove in a ground plane using higher-order boundary conditions, "IEEE Trans. Antennas Propag., vol. AP-38, no. 10, pp. 1421–1428, Sep. 1990.

[6] Park, T. J., H. J. Eom, and K. Yoshitomi, “An analysis of transverse electric scattering from a rectangular channel in a conducting plane,” Radio Science, Vol. 28, 663–673, 1993.

[7] Y. Shifman, and Y. Leviatan, "Scattering by a groove in a conducting plane a PO-MoM hybrid formulation and wavelet analysis," IEEE Trans. Antennas Propag., vol. 49, no. 12, pp. 130–136, Dec. 2001

[8] M. A. Morgan, “Mode expansion solution for scattering by a material filled rectangular groove,” Progr. Electromagn.Res., vol. PIER 18, 1998

[9] M. Bozorgi, A. Tavakoli, G. Monegato, S. H.H. Sadeghi, and R. Moini, “Backscattering from a Two Dimensional Rectangular Crack Using FIE,” IEEE Trans. Antennas Propagat., vol. 58, no. 2, pp. 552-564, Feb. 2010

[10] Cho, Y. H., "TM plane-wave scattering from finite rectangular grooves in a conducting plane using overlapping T-block method," IEEE Trans. Antennas Propagat., Vol. 54, No. 2, 746-749, 2006

[11] G. Bao, W. Sun, "A fast algorithm for the electromagnetic scattering from a large cavity,” SIAM J. Sci. Comput., vol. 27, No. 2, pp. 553-574, 2005.

[12] M. A. Basha, S. K. Chaudhuri, S. Safavi-Naein “A Fourier Expansion Solution to Plane Wave Scattering from Multiple Isosceles Right Triangle Grooves in Perfect Conducting Plane,” Photonic Applications in Devices and Communication Systems, Vol. 5970, Oct. 2005.

[13] M. A. Basha, S. K. Chaudhuri, S. Safavi-Naeini, and H. J. Eom, "Rigorous formulation for electromagnetic plane-wave scattering from a general-shaped groove in a perfectly conducting plane," J. Opt. Soc. Am. A Vol. 24, No. 6, 1647-1655, 2007.

[14] B. Alavikia, OM. Ramahi, "Finite-element solution of the problem of scattering from cavities in metallic screens using the surface integral equation as a boundary constraint,” Journal of the Optical Society of America. Vol. 26 No. 9, 1915-1925, 2009.

[15] P.L. Overfelt, D.J. White, "TE and TM modes of some triangular cross-section waveguides using superposition of plane waves,” IEEE Trans Microwave Theory Tech. Vol. 34, pp. 161–167, Jan. 1986.